Photocrosslinking-induced phase separation in evaporative solvents: formation of skin layers and microspheres

Liang Wang, Zheng Zhang and Yifu Ding*

We report the structure formation of films obtained *via* photocrosslinking of precursors during the evaporation of solvents. Although most precursor/solvent systems result in uniform dense films after the process, reaction-induced phase separation can occur in solvents with a unique combination of solubility, evaporation rate and ratio of latent heat to heat capacity. Most significantly, for such solvents, the forced convective evaporation under controlled N_2 flow results in a highly hierarchical film morphology, featuring a skin layer on top of a layer of microspheres formed *via* a nucleation and growth mechanism. For the first time, the skin layer formed during the evaporation was directly observed after the complete evaporation of the solvent. The thickness of the skin layer is dependent on the processing parameters including the N_2 flow rate, UV intensity and precursor concentrations. The skin layer formation could be suppressed by addition of non-solvent, in which case the characteristic morphology resulted from dominant spinodal decomposition. A model is presented that can qualitatively describe the skin layer formation and its dependence on the processing parameters, providing a mechanistic understanding of the photocrosslinking-induced phase separation under evaporative environments.

1 Introduction

Reaction induced phase separation (RIPS) of polymers refers to the process through which polymerization, including crosslinking of one component within a homogeneous mixture, leads to the separation between the reacting phase and the inert phase. Photoactive precursors are one classical matrix-forming system for RIPS, while the inert phase can be either organic solvents or polymers. The morphologies and, thus, physical properties of the resulting composite materials can be tailored by controlling the thermodynamic and/or kinetic factors, which has attracted broad interest from applications in liquid crystal composites,[1–3] nano to micron-sized particles,[4,5] foaming[6] and toughening of thermosets.[7,8]

When a solvent is used as the "inert" phase, its evaporation during the RIPS is normally neglected. Most often, the domains of the organic solvent are removed after the RIPS process has completed, which can be used to create porous crosslinked polymers.[9–11] In comparison, the phase evolution of photoinduced crosslinking during simultaneous solvent evaporation has been studied scarcely. Guenthner *et al.* showed that RIPS in evaporative solvents can yield sparse three-dimensional networks without significant structural collapse, which is characteristic for RIPS in non-evaporative solutions.[12]

Therefore, the coupling between photocrosslinking and fast evaporation of the solvent may lead to a plethora of film morphologies. Understanding this process can thus open an avenue for creating unique film structures, beyond that achieved in the non-evaporative solvent, and is important for applications such as solution-based photoactive coatings.

However, the interplay between photocrosslinking and solvent evaporation brings significant challenges to control the morphology using the process. Currently, the mechanistic aspect of the drying process of a non-reactive polymer solution drop has been reasonably well understood, owing to several recent studies.[13–17] One of the prominent phenomena associated with the fast drying of a polymer solution drop is the skin effect, which refers to the formation of a polymer concentrated layer at the air–solution interface. The skin layer in a non-crosslinked polymer only exists during the evaporation process and grows downwards from the air–solution surface until the vitrification of the entire film.

The goal of this study is to elaborate the mechanisms of the photocrosslinking of precursors during the fast evaporation of solvents, *via* both theoretical and systematic experimental efforts. We found that for the first time a crosslinked polymer skin layer was obtained after the process, in contrast to that occurred during the drying of non-crosslinked polymer solutions. The growth of the skin layer was interrupted by the particle-formation due to the RIPS of the solution capped underneath the skin layer. The morphologies of both the skin

Department of Mechanical Engineering, University of Colorado, Boulder, CO 80309-0427, USA. E-mail: Yifu.Ding@Colorado.edu

layer and the particle phases depend on the parameters of the photocrosslinking/evaporation process, as examined in detail.

2 Experimental

Norland® optical adhesive 65 (NOA65), a common photoactive resin, was purchased from Norland Products (Cranbury, NJ). It has been reported that this thiol–ene based adhesive resin consists of trimethylolpropane diallyl ether, trimethylolpropane tris thiol, isophorone diisocyanate ester, and benzophenone photoinitiator.[18–21] Carbon disulfide (CS_2), chloroform, toluene, and dichloromethane (DCM) were purchased from Sigma Aldrich with ACS reagent grade, ACS spectrophotometric grade, ACS reagent grade, and anhydrous grade, respectively. Tetrahydrofuran (THF), acetone, and isopropanol (IPA) were purchased from Fisher Scientific with anhydrous grade, certified ACS grade, and certified ACS plus grade, respectively. All chemicals mentioned above were used as received.

NOA65 was dissolved in a given solvent such as CS_2 at varying concentrations (by weight, unless noted otherwise). In addition to pure solvents, co-solvents consisting of a good solvent (CS_2) and a poor solvent (IPA) with varying compositions were also investigated. Note that the solvent quality, "good" or "poor", here is with regard to the NOA65 precursor instead of the crosslinked NOA. All solutions except NOA65/co-solvents were vigorously stirred until homogeneous mixtures were obtained. For the co-solvent case, NOA65 was added to a vial containing IPA and then CS_2 was slowly titrated to prevent any precipitation, according to the procedure described in ref. 12.

The photocrosslinking/evaporation process was carried out in a home-built reaction chamber that allows selectively purging N_2 to both remove the oxygen that is detrimental to some photocrosslinking reaction and to control the evaporation rate of the solvent.[22] In this study, the N_2 stream was purged for at least 5 min to saturate the reactive chamber prior to the solution deposition. Subsequently, a 100 μL solution drop was deposited onto the cover glass (untreated and air blown for 1 min) by a micropipette and immediately exposed to UV radiation for 5 min, by use of an OmniCure S2000 spot curing system with a notch filter whose bandgap is 320–500 nm. The effects of both the N_2 flow rate and UV intensity on the morphology of the films were examined.

Upon the complete removal of trapped solvents, the films were peeled off the glass slides with a razor blade and were cut into halves to examine the cross-sectional morphology of these films. A field emission scanning electron microscope (FE-SEM) (JEOL JSM-7401F) was used to measure the morphology of the films that had been coated with a thin layer of gold. The obtained SEM images were analyzed using ImageJ (National Institute of Health, USA) to estimate the thickness of the skin layer and the size of the particles resulting from the process. The skin layer thickness reported here was averaged from four measurements at different areas while the particle size, if applicable, was averaged from 30 randomly selected spheres. Furthermore, an atomic force microscope (AFM, DI 3100, Bruker) was used to examine the topography of the film surface. The measurements were performed in tapping mode under ambient conditions using silicon cantilever probes (Veeco, RTESP) with spring constants ranging between 20 and 80 N m^{-1}, as specified by the manufacturer.

## 3 Results and discussion

3.1 Experimental results for photocrosslinking of NOA65 during the evaporation of CS_2

First, a range of photoactive systems, including (meth)acrylate-based precursors, in evaporative solvents listed in Table 1, were examined. Most of these films obtained were uniform and dense, without any signs of phase separation during the process. For NOA65, photocrosslinking induced phase separation occurred during the evaporation of CS_2. The reason why the NOA65/CS_2 system displayed phase separation during evaporation and the mechanisms underlying the respective morphologies are discussed in the following. All the deposited NOA65/CS_2 solution drops were able to quickly spread over almost the entire area of the supporting glass slides (~2 cm^2), which resulted in puddle-like sessile drops, with slight curvatures in the vicinity of the three phase contact lines.[23] For a given sessile drop, the strong outward flow induced by the surface tension gradient during the solvent evaporation caused the concentrations of the precursors and/or polymers around the peripheral area to be much higher than that in the center area.[24]

As a result, transparent crosslinked films were observed near the peripheral areas for all samples, as schematically shown in Fig. 1a. In stark contrast, the solution around the central area maintained an overall low concentration of the precursors at the early stage of the process, which subsequently developed

Table 1 Important physical properties of the solvents used in the experiment[44]

	CS_2	Acetone	Chloroform	DCM	THF	Toluene	IPA
Density (g cm^{-3})	1.26	0.79	1.48	1.32	0.88	0.87	0.78
Molecular weight (g mol^{-1})	76	58	119	85	72	92	60
Solubility, δ, ((cal cm^{-3})$^{1/2}$)	10.0	10.0	9.3	9.7	9.1	8.9	11.5
Vapor pressure @21 °C (mmHg)	309	194	169	376	133	23.2	35.1
Viscosity @25 °C (cP)	0.36	0.33	0.57	0.44	0.55	0.59	2.0
Evaporation rate (butyl acetate = 1)	10.9	5.6	N/A	25	6.3	2.0	1.5
Heat of vaporization, H_v (cal mol^{-1})	6460	7076	7021	6715	6664	7985	9540
Specific heat, C_p (cal mol^{-1} K^{-1})	18	30	27	24	36	41	37
H_v/C_p	359	236	260	280	185	195	258
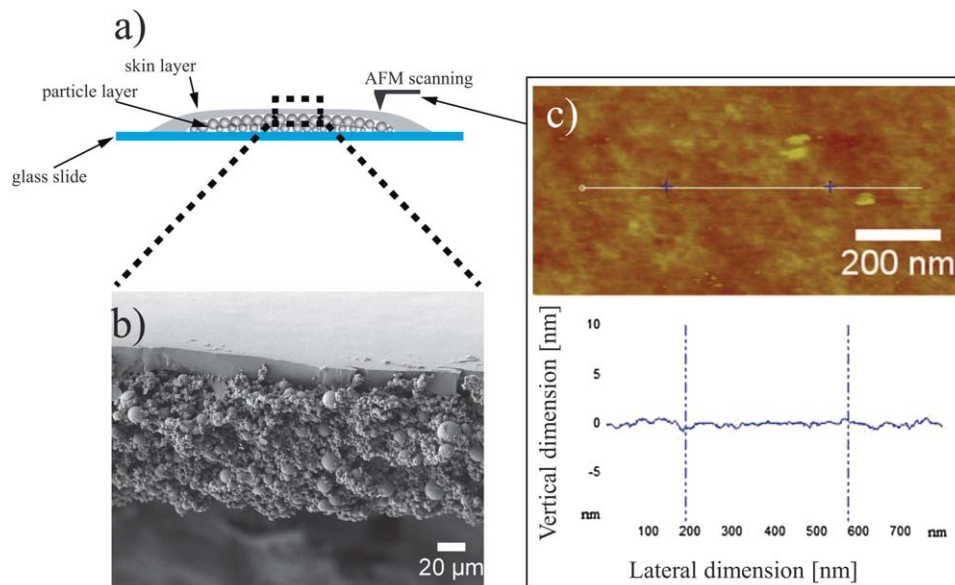
Fig. 1 (a) Schematic illustration of the typical hierarchical structure of films formed by photocrosslinking of NOA65 during the evaporation of CS_2. (b) Representative SEM image of the cross-section of the film, showing a smooth skin layer on top of a particle layer. (c) Topographic AFM image of the skin layer (top) and the corresponding cross-sectional profile (bottom). The processing parameters for this representative sample are: 10% NOA65 in CS_2, a UV intensity of 50 mW cm^{-2}, and a N_2 flow rate of 1 L min^{-1}.

into a hierarchical morphology as illustrated in Fig. 1a. In this study, we focus on the morphology at the central area of the films, where the photocrosslinking and mass transfer are highly coupled while the lateral mass transfer is not dominant.

As schematically illustrated in Fig. 1a, the crosslinked NOA65 films obtained from photocrosslinking during the CS_2 evaporations were often composed of two distinctive structural features: a crosslinked dense skin layer on top of a crosslinked micron-sized particle layer. Fig. 1b shows a representative cross-sectional SEM image of a NOA65 film, revealing such a hierarchical structure. The thickness of the skin layer was relatively uniform, and the interface between the skin layer and the particle layer appeared to be sharp (Fig. 1b). The air-side surface of the skin layer was smooth, with an RMS roughness of less than 5 nm, according to the AFM measurements (Fig. 1c). The thicknesses of these layers as well as the size and distribution of the particles were highly dependent on the processing conditions, which is described in detail in the following. Note that the SEM images do not reveal the overall thickness of the films (skin layer plus the microsphere layers) as some microsphere layers were left on the glass slides side when we peeled the films off.

First, we examined the influence of the N_2 flow rate on the final morphology of the films. Fig. 2 shows the cross-sectional images of the photo-crosslinked NOA65 films obtained under N_2 flow rates ranging from 0 to 5 L min^{-1}. When the N_2 flow rate was 0, *i.e.* the evaporation of CS_2 was free convection, the skin layer was hardly discernible and appeared granular (inset of Fig. 2a). From the top to the bottom of the film, a particulate structure was observed: the particles were tightly connected and displayed a uniform distribution in size (diameter $\sim$ 2.5 μm). This type of a particulate morphology sometimes is referred to as "connected-globule" or "string of pearls" structure, which

might have resulted from phase separation *via* a classical spinodal decomposition (SD) mechanism.[8,25]

Once the polymerization of the precursors pushed the mixture into the unstable region of the phase diagram, concentration waves occurred spontaneously. The fastest growing wave, with a wavelength of Λ_m (a function of quench depth), became the dominant structure. Normally, one of the two continuous phases, namely polymer-rich and solvent-rich, broke into droplets due to the interfacial fluctuations. Hence, the uniform particle size was reminiscent of the dominant spinodal wavelength Λ_m. Because the particles were (partially) crosslinked during the phase separation, the subsequent coalescence of the particles was limited. Furthermore, the higher resolution SEM image (inset of Fig. 2a) revealed that all of these particles were wrinkled. This phenomenon is consistent with the SD process. The effective concentration in both of the continuous phases kept evolving towards equilibrium, meaning that even after the phase separation, there was appreciable solvent left within the crosslinking polymer phase. The volume shrinkage of these crosslinked particles during the final evaporation of these solvents can induce such wrinkled structures.[26]

Under controlled N_2 flow rates, the structures of the films were similar, consisting of a skin layer and a particulate layer (Fig. 2b–d), both of which were different from those found in films without N_2 flow (Fig. 2a). The skin layers were extremely smooth on the air-surface side, and the interfaces were sharp between the skin layers and the particulate layers (Fig. 2b–d). Correspondingly, the thickness of the skin layers increased from 17, 19 to 27 μm, as the N_2 flow rates increased from 1, 3, to 5 L min^{-1}. In contrast, the morphology of the particulate layers for films obtained under different N_2 flow rates appeared nearly identical. These microspheres were more spherical, less
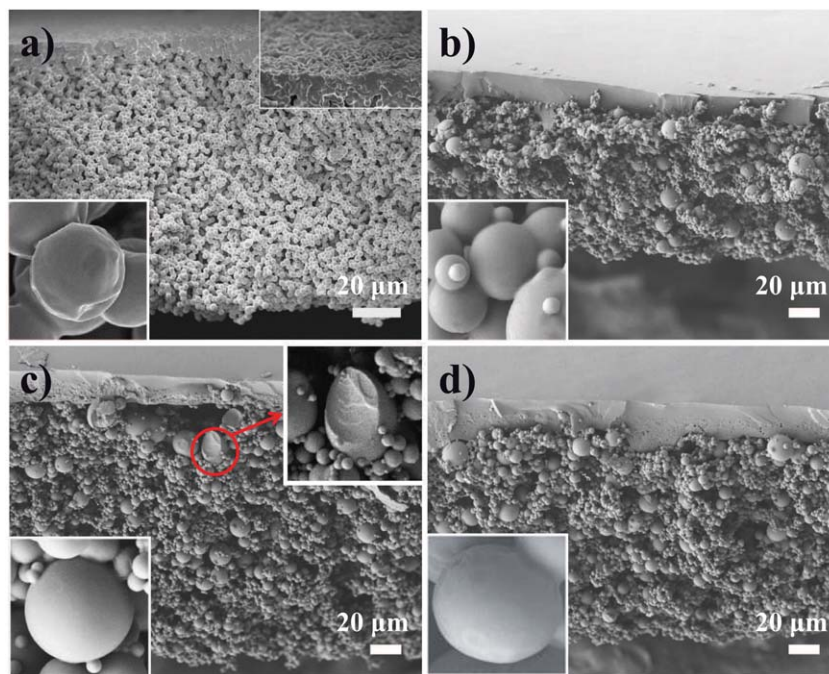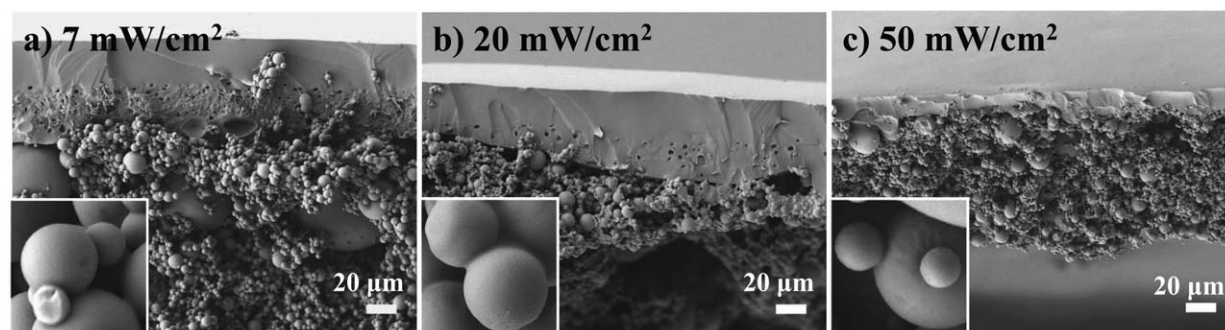
Fig. 2 Cross-sectional SEM images of the crosslinked films prepared with 10% NOA65 in CS_2 under an UV radiation intensity of 50 mW cm^{-2} at varying N_2 flow rates: (a) 0 L min^{-1}, (b) 1 L min^{-1}, (c) 3 L min^{-1}, and (d) 5 L min^{-1}. The inset in the upper right of (a) is the magnified view of the top surface of the skin layer, and of (c) is the magnified view of the cross-section of the fractured particle. The insets shown at the lower left corners of (a–d) are the magnified view of individual particles.

connected, and had broader distributions in sizes, compared with the ones in Fig. 2a. None of these particles showed wrinkles on the outer shell (insets of Fig. 2b–d).

All these morphological features suggest that these particles were a result of phase separation *via* the nucleation and growth (NG) mechanism. Due to the random nucleation in the solution, the crosslinked polymer particles had a broad distribution in size (sub-microns to tens of microns) caused by the difference in their nucleation time, and were not tightly connected together. The composition of these spheres, once nucleated, reached nearly the equilibrium composition, containing very low concentrations of solvent (CS_2). Thus the volume shrinkages of these particles were small when CS_2 diffused out during the complete drying of the films, which did not lead to any wrinkling of the particle shells. From the microsphere that was

accidentally fractured during the cross-sectioning of the film (upper right inset of Fig. 2c), the sphere was nearly solid, confirming that there were no pores left due to the entrapped CS_2 domains.

Fig. 3a–c present the SEM images of the cross-sections of the films obtained under a constant N_2 flow rate (1 L min^{-1}) but varying UV intensities. The overall film morphologies were similar to those obtained in Fig. 2b–d. However, the variation of UV intensity had a stronger effect on the thickness of the skin layer than the N_2 flow rate, within the range studied. Specifically, the thickness of the skin layer decreased from 72, 52, to 15 μm as the intensities of the UV radiation increased from 7, 20, to 50 mW cm^{-2}, correspondingly. For all three samples, the particulate layers clearly showed a NG type of phase separation mechanism, similar to that discussed above.

Fig. 3 Cross-sectional SEM images of crosslinked films prepared with 10% NOA65 in CS_2 at a N_2 flow rate of 1 L min^{-1} under varying UV intensities: (a) 7 mW cm^{-2}, (b) 20 mW cm^{-2}, and (c) 50 mW cm^{-2}. The insets at the lower left corners of (a–c) are the magnified view of selected individual particles.

The samples obtained under 7 mW cm^{-2} UV radiation intensity showed the broadest distribution in particle size among the three (Fig. 3a).

Fig. 4a–d show the cross-sectional morphologies of the films prepared using NOA65/CS$_2$ solutions containing a NOA65 fraction of 1%, 5%, 10%, and 40%, respectively. For 1–10% NOA65/CS$_2$ solutions, the morphologies of the films were similar to the above discussed ones. The skin layer thickness increased from 2.4, 6.4, to 16 μm as the concentration of NOA65 in the solution increased from 1%, 5% to 10%. The structural characteristics of the microspheres indicate that the governing mechanism for forming these spheres was NG. However, for the solution containing 40% NOA65 precursor, the photocrosslinked film showed no morphological signs of RIPS, but rather a dense crosslinked film (Fig. 4d).

3.2 Mechanism for the formation of the skin layer and the particulate layer

A theoretical interpretation of the skin layer during the fast drying of a polymer solution was reported by de Gennes.[27] Doi and co-workers proposed an analytic model to describe the criterion for the formation of a skin layer and its growth rate.[17,28,29] Alongside these theoretical efforts, Pauchard and Allain experimentally investigated the buckling instability on the skin layer during the drying of a polymer solution.[30,31] Despite these efforts, the nature of the skin layer, with regard to whether it is a gelled or vitrified state, remains unclear. It is challenging to directly measure the polymer skin layer either *ex situ* or *in situ* during the solvent evaporation, because of the re-dissolution and/or low mechanical strength of the uncrosslinked polymers. Until recently, Shimokawa *et al.* measured the skin layer during the early stage of the evaporation by combining the electric field tweezers with an optical lever technique using parallel-lined laser beams.[32] For the first time, the growth rate of the skin layer for polyvinyl acetate (PVAc) and polymethyl methacrylate (PMMA) solutions as a function of time, as well as their stiffness, was determined.[33]

For the process of interest here, namely, photocrosslinking of precursors during the evaporation of a volatile solvent, crosslinked skin layers were observed for the first time (Fig. 1–4), which remained in the final film morphology. Note that the formation of the crosslinked skin layer did not prevent the continuous evaporation of the solvent, similar to that in the non-reactive system. The solvent can readily diffuse through the swollen skin layer into the vapor phase. Here, we describe the mechanistic aspects of the skin layer formation in such a dynamic system by modifying the current theoretical descriptions of a non-crosslinked polymer solution.

Fig. 5 illustrates the height (or thickness) of the solution puddle as a function of processing time. The quick evaporation of the solvent, aided by the convective mass transfer, cannot be balanced by the solvent diffusion and causes a steep concentration gradient of monomers (or oligomers) near the solution–air interface. Under UV radiation, this concentrated monomer layer polymerizes/crosslinks rapidly *via* the free-radical mediated step-growth polymerization of NOA65, resulting in a gelled/vitrified skin layer at the surface. The thickness of the layer grows from the air–solution surface downwards into the solution by coagulating/polymerizing with adjacent monomers/oligomers. In the following, we derive the growth rate of this crosslinked skin-layer.
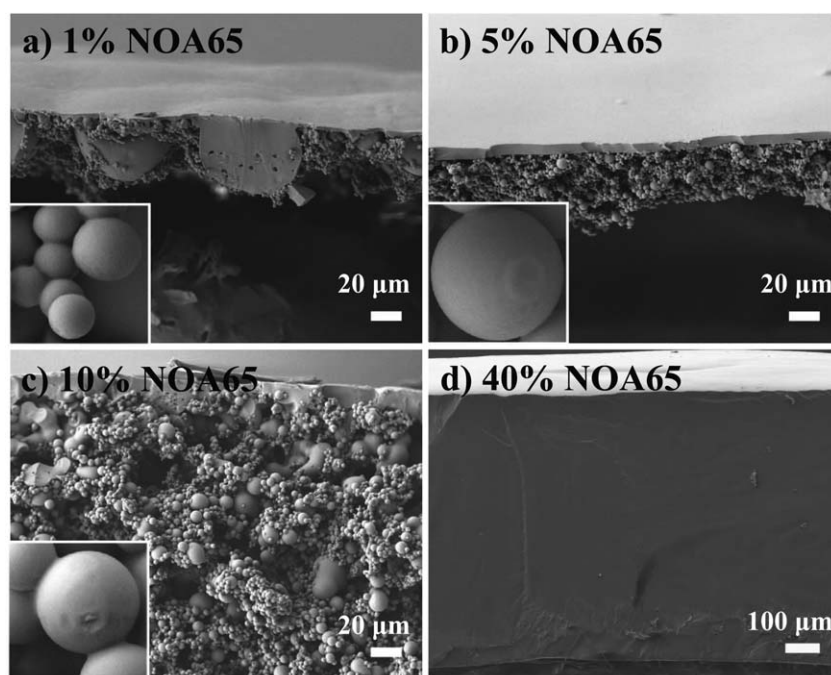
Fig. 4 Cross-sectional SEM images of crosslinked films prepared at a N$_2$ flow rate of 1 L min^{-1} under a UV intensity of 50 mW cm^{-2}, with varying initial concentrations of NOA65: (a) 1%, (b) 5%, (c) 10%, and (d) 40%. The insets shown at the lower left corners of (a–c) are the magnified view of selected individual particles.
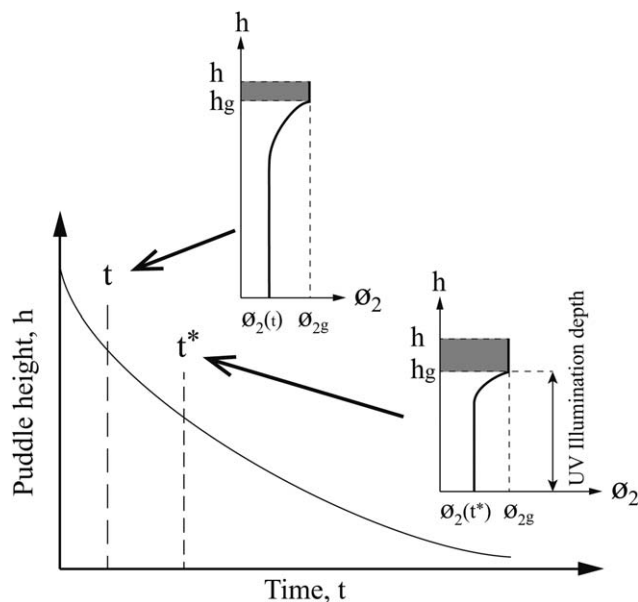
Fig. 5 Schematic illustration of the evolution of puddle height as a function of drying time. The insets show the concentration profiles of the precursor/polymers at different times.

We start by examining the mass transfer at the top surface of the evaporating solution drop. The Reynolds number (Re) of the N_2 flow over the solution drop in the reaction chamber can be estimated by assuming that the N_2 flow velocity approaching the leading edge of the glass substrate was approximately equal to the inlet velocity (diameter of the inlet pipe is 4.43 mm). Re can be estimated for a given N_2 flow rate (V) used, $Re = VL/\nu$, where L is the length of the casting glass substrate in the flow direction and ν is the kinematic viscosity. Quantitatively, Re varied between ~1600 and ~8000 for the different N_2 flow rates used, which indicates that the flow was dominantly laminar.[34] Therefore, the average mass transfer coefficient for laminar flow, $\overline{k_c}$, can be extracted from Sherwood number,

$$Sh_L = \frac{\overline{k_c}L}{D_{AB}} = 0.664 Re^{1/2} S_c^{1/3} \tag{1}$$

where D_{AB} is the diffusion coefficient of CS_2 into N_2 and $S_c = \nu/D_{AB}$ is the Schmidt number, manifested as the ratio of momentum diffusivity to mass diffusivity. Thus, $\overline{k_c}$ is a constant for a given N_2 flow rate. We can now estimate the evaporation flux of the solvent, J, by

$$J = \overline{k_c}\left(c_{1g} - c_{1\infty}\right) \tag{2}$$

where c_{1g} and $c_{1\infty}$ are the concentration of solvent just above the air–solution interface and at a distance infinitely far away from solution, respectively. $c_{1\infty}$ can be assumed to be zero. Applying the ideal gas law, $c_g = p_g/RT$, where p_g is the partial vapor pressure of solvent right above the interface, we have

$$J = \frac{\overline{k_c}\,p_g}{RT} \tag{3}$$

Local equilibrium at the free surface of a solution drop can be established by applying Henry's law,

$$\frac{p_g}{p_v} = \Phi_{1h} = 1 - \Phi_{2h} \tag{4}$$

where p_v is the vapor pressure of the pure solvent. Combining eqn (3) and (4), we have,

$$J = \frac{\overline{k_c}\,p_v}{RT}\left(1 - \Phi_{2h}\right) \tag{5}$$

Now, we can estimate the growth rate of the top skin layer, r_{skin}, by incorporating eqn (5) into Doi's model,[17]

$$r_{skin} = \dot{h} - \dot{h}_g = \frac{\overline{k_c}\,p_v}{RT}\frac{\Phi_{2i}\left(1 - \Phi_{2g}\right)}{\Phi_{2g} - \Phi_{2i}} \tag{6}$$

where $\dot{h}$ is the velocity of the solution surface boundary, $\dot{h}_g$ is the velocity of the interface between the remaining solution and the skin layer, Φ_{2i} is the initial monomer volume fraction, and Φ_{2g} is the critical monomer or polymer fraction above which the skin layer is formed. Here we assume that Φ_{2g}, p_v and T are constants for all processing conditions, although p_v is indeed a function of T that is also dependent on the varying external airflow.[35]

In non-crosslinked polymer solution, the growth of the skin layer continues until the entire film turns into a gelled/vitrified state, resulting in a uniform dried film. The skin layer cannot be extracted, because once the evaporation of the solvent is stopped, the skin layer will be re-dissolved. However, for the photocrosslinking of monomers during the solvent evaporation, the skin layer growth can be interrupted, and the skin layer be obtained without the re-dissolution due to the crosslinking. Here, the process that limits the growth of the skin layer is the RIPS of the remaining solution capped underneath the skin layer, as schematically drawn in Fig. 5.

The instantaneous thermodynamics of the reacting solution can be expressed as,[36,37]

$$\frac{\Delta\mu_1}{RT} = \ln a_1 = \ln(1 - \Phi_2) + \Phi_2\left(1 - \frac{1}{x}\right) + \chi\Phi_2^2 + v_e\overline{V_1}\left(A(\Phi_{2n})^{2/3}\Phi_2^{1/3} - B\Phi_2\right) \tag{7}$$

where $\Delta\mu_1$ is the chemical potential change of solvent after mixing, a_1 is the activity of the solvent, Φ_{2n} equals to the volume fraction of the polymer at network formation, χ is the Flory–Huggins interaction parameter, x is the ratio of molar volumes of the polymers to solvent, v_e is the concentration of elastically active network chains in a volume unit, $\overline{V_1}$ is the molar volume of the solvent, and A and B are front factors depending on the specific network models. Note that the last term in eqn (7) only contributes to the solvent activity when the three dimensional network has already formed. Eqn (7) reveals that Φ_2 negatively contributes to the change of solvent activity, whereas x positively.

All the organic components in the solution (solvent, precursors, and polymers formed) absorbed UV radiation, therefore, limiting its penetration depth.[38–40] At the early stage of the evaporation, the entire solution of the puddle was "optically thick" and only a thin portion of the solution near the surface was "activated." For this thin region near the top surface, the increase in a_1 due to the molecular buildup (x) was balanced by a rapid mass loss of solvent due to the evaporation

(Φ_2). Therefore, no phase separation took place, and a gelled skin layer was formed. In other words, as the polymerization moved the phase diagram up, the fast evaporation of the solvent kept the effective concentration increased and remained in the one-phase region. As mentioned earlier, at the peripheral region of the deposited droplet, the crosslinked films obtained were also transparent, as a result of the significantly high concentration of monomers/polymers due to the strong outward flow.

Once the skin layer formed, the evaporation rate in the bulk solution was slowed down, meaning that the solution capped beneath the skin layer did not have a strong concentration gradient (Fig. 5).[30,41,42] During this stage, the skin layer kept growing and the particulate-morphology started to form via the NG. Once the solution puddle became "optically thin", the UV radiation induced a crosslinking reaction in the entire capped solution (Fig. 5). In this case, the increase of molecular weight (x) dominated the mixing free energy of the system, as Φ_2 remained low, which caused a net gain of solvent activity (eqn (7)). In other words, polymerization moved the phase diagram of the solution up, while the overall concentration was kept rather constant. Furthermore, the evaporation of the solvent caused the temperature of the solution to drop appreciably. Due to both the photo-crosslinking reaction and the cooling effect of the solvent evaporation, RIPS occurred within the solution entrapped by the skin layer and led to the observed particulate layers. It appears that for all the samples that formed the skin layer, NG was the dominant mechanism for the RIPS.

Most significantly, the RIPS in the capped solution effectively imposes a finite time, t^*, to the skin layer growth, which determines the thickness (b) of the crosslinked skin layer,

$$b = \int_0^{t^*} r_{skin} dt = \frac{\overline{k_c} p_v}{RT} \frac{\Phi_{2i}(1 - \Phi_{2g})}{\Phi_{2g} - \Phi_{2i}} t^* \quad (8)$$

Therefore, the formation of the hierarchical structure was dictated by the competition between solvent evaporation and RIPS induced by photocrosslinking. Dayal and Kyu reported that by controlling the relative rates of solution evaporation to phase separation in polymer solution, fiber morphologies including skin-core, uniform fiber surface with phase separated core, and porous fiber can be readily obtained.[43] In the current system, RIPS is used to limit the skin layer thickness rather than the traditional phase separation. In the following, we use the theoretical framework obtained in eqn (8) to elaborate the influence of processing parameters on the different film morphologies observed in Fig. 2–4.

A higher N_2 flow rate leads to a larger $\overline{k_c}$, which in turn produces a higher growth rate of the skin layer and finally a thicker skin layer (eqn (8)). Note that t^* might decrease with an increase of the flow rate, i.e. the time scale for the RIPS to set-in in the remaining solution is shorter. Nonetheless, the observed slight increase of skin layer thickness with an increase of the N_2 flow rate (Fig. 2) suggests that the growth rate is more dominant (eqn (8)). When the N_2 flow rate is zero, the concentration gradient at the solution surface is low, i.e. diffusion of solvent can more or less balance the loss of solvent caused by

evaporation. Therefore, effectively, no skin layer is formed. Instead, the overall concentration of the puddle remains rather homogeneous and increases over time. Finally, RIPS of the entire solution gave rise to the connected-globule morphology (Fig. 2a). Studies by Sharma et al. have shown that the temperature of the solution decreases with the decrease of the evaporation rate, counterintuitively.[35] Therefore, the phase separation of the colder solution without N_2 flow is more likely to occur in the unstable region (the SD mechanism), while that of the other solutions under N_2 flow occur in the metastable region (the NG mechanism).

At a fixed N_2 flow rate, the growth rate of the skin layer of a given solution is constant (eqn (6)), and the thickness of the skin layer is thus dependent on the growth time, t^*. With the increase of UV intensity, both the illumination depth and the crosslinking rate in the trapped solution increase, which reduces t^*. Hence, the skin layer thickness decreases with the increase of UV intensity according to eqn (8), which was indeed experimentally observed (Fig. 3).

At both constant N_2 flow rate and UV intensity, the skin layer formation also depends on the initial concentration of the precursors. Eqn (6) clearly predicts that an increase in Φ_{2i} results in an increase of growth rate of the skin layer, in the range of $0 < \Phi_{2i} < \Phi_{2g}$. Furthermore, the mass loss of solvent in more concentrated solution is slower, resulting in longer t^* for the growth of the skin layer. Both factors suggest that an increase of the initial precursor concentration would lead to an increase in skin layer thickness (eqn (8)), which is consistent with the experimental findings (Fig. 4). For the 40% NOA65 solution, no phase separated structure was observed throughout the film, suggesting that the solution capped beneath the skin layer did not enter the two-phase region of the phase diagram, due to its high concentration.

3.3 Influence of solvent and co-solvents on the film morphology

Besides CS_2, five other volatile solvents with 10% NOA65 were examined including acetone, chloroform, DCM, THF and toluene, whose relevant properties are listed in Table 1. The UV intensity was 50 mW cm^{-2}, with 1 L min^{-1} N_2 flow rate. For all five solvents, the obtained NOA65 films were transparent and dense, with no phase separated structures. The miscibility between the solvent and the polymerizing NOA65 is often related to the solubility parameters (δ) of the components. For CS_2 and acetone, δ ($\sim$10 (cal cm^{-3})$^{1/2}$) is higher than the other 4 solvents used, but smaller than IPA (Table 1). As previously noted, IPA is a non-solvent even for the uncrosslinked NOA65.[12] Therefore, solvents with smaller δ favor the mixing with the NOA65, and no phase separation was observed for chloroform, DCM, THF and toluene.

Although acetone has an identical δ to CS_2, the miscibility of the acetone with NOA65 is further dependent on the temperature of the evaporating solution. The evaporation of the solvent causes the cooling of the solution drop, and the degree of temperature drop in the solution is determined by both the latent heat (H_v) and the heat capacity (C_p) of the solvent. The

ratio of H_v/C_p for CS_2 is ~50% higher than that of acetone, suggesting that the cooling of CS_2 is much more dramatic than acetone at the same concentration. Furthermore, the process can be considered adiabatic only when the evaporation rate is very high, meaning that less heat loss to the environment at a higher evaporation rate. As listed in Table 1, the evaporation rate of CS_2 (in reference to butyl acetate) is ~100% higher than that of acetone. Both factors (faster evaporation and higher H_v/C_p) caused the effective temperature of CS_2 solution to be much lower than that of the acetone solution. Therefore, despite the polymerization of NOA65, the acetone solution/mixture remained in the one phase region for the UCST phase diagram, and no RIPS occurred.[12]

At last, we examined the co-solvent, by mixing IPA with CS_2. IPA is a non-solvent for NOA65, even prior to the polymerization,[12] which was confirmed experimentally from the phase separation in NOA65/IPA after vigorous mixing. Co-solvents containing 10%, 30%, and 50% IPA in the total solution were investigated. Note that since the NOA65 concentration was kept constant at 10%, CS_2 concentrations in the solution were 80%, 60%, and 40%, correspondingly. All the three IPA/CS_2 co-solvents were able to dissolve the NOA65 precursors. Fig. 6 shows the cross-sectional morphology of the films obtained from photocrosslinking under the evaporation of the IPA/CS_2 co-solvents. The film that resulted from a co-solvent with 10% IPA showed that the majority of the film from the top surface was solid and dense (Fig. 6a-1). Near the bottom (in contact with the glass substrate), some phase separated structures were evident (indicated by the arrow in Fig. 6a-1, and amplified in Fig. 6a-2). However, these structures indicate that the phase separation was frozen at the early stage of the RIPS.

As the IPA composition increased to 30%, a characteristic "connected-globule" structure of crosslinked NOA65 was observed (Fig. 6b-1 and b-2). The average diameter of the crosslinked NOA65 "particles" was ~890 nm. With the IPA composition in the solution further increased to 50%, a similar morphology was observed with smaller NOA65 "particles" (~560 nm) (Fig. 6c-1 and c-2). For both 30% and 50% IPA, no skin layers were observed in the final films. This trend is consistent with that observed in Fig. 2a: SD-dominated phase separation occurred in the absence of skin layers. The smaller NOA65 particle size in higher IPA concentration could result from the larger "quenching depth" in the phase diagram that predicts a smaller Λ_m.[25] At present, it remains unclear why the skin layer did not form in the tertiary systems, during the forced convective evaporations of the two solvents.

4   Conclusions

Here we investigate the morphology of films formed by photo-crosslinking of NOA65 precursors within evaporative solvents. With the free-convective evaporation of the solution, the RIPS of NOA65 occurred *via* the SD process, resulting in a classical connected-globule structure. Under the forced-convective evaporation using N_2 flow, a hierarchical morphology was observed, featuring a skin layer on top of a micron-sized particulate layer formed *via* NG. For the first time, the polymer skin layer formed during the evaporation can be obtained after the evaporation, in contrast to the linear polymer solutions. The final thickness of the skin layer is dependent on the processing parameters ranging from the N_2 flow rate, UV intensity to NOA65 concentration. A theoretical model, based on the one for
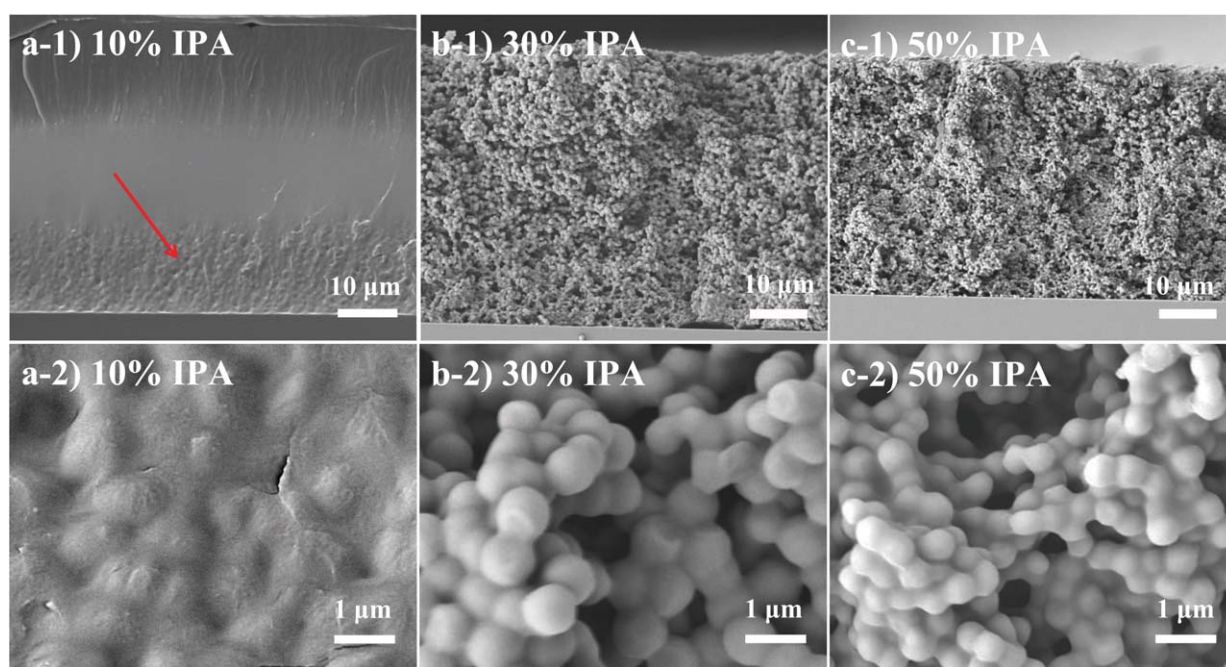
Fig. 6   Cross-sectional SEM images of crosslinked NOA65 films, using IPA and CS_2 as co-solvents, the respective IPA to CS_2 ratios were: (a-1) 1 : 8, (b-1) 3 : 6, and (c-1) 5 : 4. (a-2), (b-2) and (c-2) are the magnified view of (a-1), (b-1), and (c-1). The NOA65 concentration was kept constant at 10%, while the UV intensity and N_2 flow rate were 50 mW cm^{-2} and 1 L min^{-1}, correspondingly.

the non-crosslinked polymer solution, is developed that can successfully describe the skin layer formation and its dependence on these processing parameters. A comparison with other volatile solvents shows that CS_2 is a unique solvent to achieve this type of hierarchical structures of NOA65, owing to the combination of the solubility parameter, fast evaporation, and large value of H_v/C_p. Furthermore, by adding IPA (non-solvent for NOA65) into CS_2, the skin layer formation was suppressed, and the SD-induced structures became dominant.

Our study suggests that, whenever a skin layer forms for photocrosslinking in an evaporative environment, the entrapped solution will undergo a NG mechanism for the subsequent RIPS and result in microspheres with a broad distribution of sizes. If the skin layer formation is suppressed by controlling the processing parameters, then the RIPS of the solution will most likely occur *via* SD because of its broader window in the phase diagram, and result in connected particles with uniform sizes. These findings provide a mechanistic understanding of the photocrosslinking process under evaporative environments, which is important for its potential applications such as photoactive coatings, separation membranes and drug delivery.

Acknowledgements

References

1 D. Nwabunma, K. J. Kim, Y. Lin, L. C. Chien and T. Kyu, *Macromolecules*, 1998, **31**, 6806–6812.

2 V. Vorflusev and S. Kumar, *Science*, 1999, **283**, 1903–1905.

3 T. Qian, J. H. Kim, S. Kumar and P. L. Taylor, *Phys. Rev. E*, 2000, **61**, 4007–4010.

4 M. Traina, J. Galy, J. F. Gérard, T. Dikic and T. Verbrugge, *J. Colloid Interface Sci.*, 2012, **368**, 158–164.

5 J. S. Downey, G. McIsaac, R. S. Frank and H. D. H. Stöver, *Macromolecules*, 2001, **34**, 4534–4541.

6 W. Li, A. J. Ryan and I. K. Meier, *Macromolecules*, 2002, **35**, 5034–5042.

7 S. K. Siddhamalli and T. Kyu, *J. Appl. Polym. Sci.*, 2000, **77**, 1257–1268.

8 K. Yamanaka and T. Inoue, *Polymer*, 1989, **30**, 662–667.

9 J. Kiefer, J. G. Hilborn, J. A. E. Månson, Y. Leterrier and J. L. Hedrick, *Macromolecules*, 1996, **29**, 4158–4160.

10 Y. Luo, K. Cheng, N. Huang, W. Chiang and S. Li, *J. Polym. Sci., Part B: Polym. Phys.*, 2011, **49**, 1022–1030.

11 O. Okay, *Prog. Polym. Sci.*, 2000, **25**, 711–779.

12 A. J. Guenthner, D. M. Hess and J. J. Cash, *Polymer*, 2008, **49**, 5533–5540.

13 M. Tsige and G. S. Grest, *Macromolecules*, 2004, **37**, 4333–4335.

14 H. Hu and R. G. Larson, *Langmuir*, 2005, **21**, 3963–3971.

15 H. Hu and R. G. Larson, *Langmuir*, 2005, **21**, 3972–3980.

16 H. Hu and R. G. Larson, *J. Phys. Chem. B*, 2002, **106**, 1334–1344.

17 T. Okuzono, K. Ozawa and M. Doi, *Phys. Rev. Lett.*, 2006, **97**, 136103.

18 G. W. Smith, *Mol. Cryst. Liq. Cryst.*, 1991, **196**, 89–102.

19 R. Benmouna and B. Benyoucef, *J. Appl. Polym. Sci.*, 2008, **108**, 4072–4079.

20 J. B. Nephew, T. C. Nihei and S. A. Carter, *Phys. Rev. Lett.*, 1998, **80**, 3276–3279.

21 L. Dolgov, O. Yaroshchuk and L. Qiu, *Mol. Cryst. Liq. Cryst.*, 2007, **468**, 687–696.

22 L. Wang, S. H. Maruf, D. Maniglio and Y. Ding, *Polymer*, 2012, **53**, 3749–3755.

23 P. G. de Gennes, F. Brochard-Wyart and D. Quere, *Capillarity and wetting phenomena: drops, bubbles, pearls, waves*, Springer, Berlin, 2003.

24 T. Kajiya, D. Kaneko and M. Doi, *Langmuir*, 2008, **24**, 12369–12374.

25 T. Inoue, *Prog. Polym. Sci.*, 1995, **20**, 119–153.

26 B. Li, Y. Cao, X. Feng and H. Gao, *Soft Matter*, 2012, **8**, 5728–5745.

27 P. G. de Gennes, *Eur. Phys. J. E: Soft Matter Biol. Phys.*, 2002, **7**, 31–34.

28 T. Okuzono and M. Doi, *Phys. Rev. E: Stat., Nonlinear, Soft Matter Phys.*, 2008, **77**, 030501.

29 K. Ozawa, T. Okuzono and M. Doi, *Jpn. J. Appl. Phys.*, 2006, **45**, 8817–8822.

30 L. Pauchard and C. Allain, *Europhys. Lett.*, 2003, **62**, 897–903.

31 L. Pauchard and C. Allain, *Phys. Rev. E: Stat., Nonlinear, Soft Matter Phys.*, 2003, **68**, 052801.

32 Y. Shimokawa, T. Kajiya, K. Sakai and M. Doi, *Phys. Rev. E: Stat., Nonlinear, Soft Matter Phys.*, 2011, **84**, 051803.

33 S. Arai and M. Doi, *Eur. Phys. J. E: Soft Matter Biol. Phys.*, 2012, **35**, 57.

34 H. D. Baehr and K. Stephan, *Heat and Mass Transfer*, Springer, Berlin Heidelberg, 2006.

35 V. Sharma, L. Song, R. L. Jones, M. S. Barrow, P. R. Williams and M. Srinivasarao, *Europhys. Lett.*, 2010, **91**, 38001.

36 K. Dušek and M. Dušková-Smrčková, *Prog. Polym. Sci.*, 2000, **25**, 1215–1260.

37 M. Dušková-smrčková and K. Dušek, *J. Mater. Sci.*, 2002, **37**, 4733–4741.

38 J. A. Burdick, A. J. Peterson and K. S. Anseth, *Biomaterials*, 2001, **22**, 1779–1786.

39 A. K. O'Brien and C. N. Bowman, *Macromolecules*, 2003, **36**, 7777–7782.

40 J. A. Burdick, T. M. Lovestead and K. S. Anseth, *Biomacromolecules*, 2003, **4**, 149–156.

41 T. Kajiya, E. Nishitani, T. Yamaue and M. Doi, *Phys. Rev. E: Stat., Nonlinear, Soft Matter Phys.*, 2006, **73**, 011601.

42 N. Tso, MSc thesis, Ohio University, 1984.

43 P. Dayal and T. Kyu, *J. Appl. Phys.*, 2006, **100**, 043512.

44 I. M. Smallwood, *Handbook of organic solvent properties*, Elsevier, 1996.